



**HAL**  
open science

## Production and Characterization of Oxyhydroxyapatites

Liene Pluduma, Karlis Agris Gross, Christian Rey, Arnolds Ubelis, Astrida Berzina

► **To cite this version:**

Liene Pluduma, Karlis Agris Gross, Christian Rey, Arnolds Ubelis, Astrida Berzina. Production and Characterization of Oxyhydroxyapatites. Key Engineering Materials, 2018, 762, pp.48-53. 10.4028/www.scientific.net/KEM.762.48 . hal-02329364

**HAL Id: hal-02329364**

**<https://hal.science/hal-02329364>**

Submitted on 23 Oct 2019

**HAL** is a multi-disciplinary open access archive for the deposit and dissemination of scientific research documents, whether they are published or not. The documents may come from teaching and research institutions in France or abroad, or from public or private research centers.

L'archive ouverte pluridisciplinaire **HAL**, est destinée au dépôt et à la diffusion de documents scientifiques de niveau recherche, publiés ou non, émanant des établissements d'enseignement et de recherche français ou étrangers, des laboratoires publics ou privés.




## Open Archive Toulouse Archive Ouverte (OATAO)

OATAO is an open access repository that collects the work of Toulouse researchers and makes it freely available over the web where possible

This is an author's version published in: <http://oatao.univ-toulouse.fr/24529>

**Official URL:** <https://doi.org/10.4028/www.scientific.net/KEM.762.48>

**To cite this version:**

Pluduma, Liene and Gross, Karlis Agris and Rey, Christian  and Ubelis, Arnolds and Berzina, Astrida *Production and Characterization of Oxyhydroxyapatites*. (2018) Key Engineering Materials, 762. 48-53. ISSN 1662-9795

Any correspondence concerning this service should be sent to the repository administrator: [tech-oatao@listes-diff.inp-toulouse.fr](mailto:tech-oatao@listes-diff.inp-toulouse.fr)

## Production and Characterization of Oxyhydroxyapatites

Liene Pluduma<sup>1,a\*</sup>, Karlis Agris Gross<sup>1,b</sup>, Christian Rey<sup>2,c</sup>, Arnolds Ubelis<sup>3,d</sup>  
and Astrida Berzina<sup>4,e</sup>

<sup>1</sup>Institute of Inorganic Chemistry, Riga Technical University, Latvia

<sup>2</sup>ENSIACET, University of Toulouse, France

<sup>3</sup>Institute of Atomic Physics and Spectroscopy, University of Latvia, Latvia

<sup>4</sup>Institute of Technical Physics, Riga Technical University, Latvia

<sup>a</sup>liene.pluduma@rtu.lv, <sup>b</sup>kgross@rtu.lv, <sup>c</sup>christian.rey@ensiacet.fr, <sup>d</sup>arnolds@latnet.lv,  
<sup>e</sup>astrida.berzina@rtu.lv

**Keywords:** hydroxyapatite, oxyhydroxyapatite, oxyapatite, hydroxyl ions, fourier transform infrared spectroscopy, deconvolution

**Abstract.** The amount and alignment of hydroxyl ions influence the bioactivity of hydroxyapatite. Hydroxyl ions in hydroxyapatite are the most mobile and upon heating are the first to leave the lattice to form oxyhydroxyapatite. This work describes a method for producing hydroxyapatite with different amounts of hydroxyl ions, and reports on the changes in Fourier transform infrared absorption at increasing level of dehydroxylation. Detailed analysis of spectra in the 500-700 cm<sup>-1</sup> range showed a peak shift for the hydroxyl ion absorption line at 632 cm<sup>-1</sup> to 637 cm<sup>-1</sup> and an increase in the wavenumber for the phosphate line at 575 cm<sup>-1</sup>.

### Introduction

Hydroxyapatite (HA, Ca<sub>10</sub>(PO<sub>4</sub>)<sub>6</sub>(OH)<sub>2</sub>) is widely used as a ceramic or coating for biomaterial applications. Considerable work has been conducted on altering the amount of calcium and phosphorous in the material as well as substitutions for calcium, but the detection and alterations of the hydroxyl ions (OH<sup>-</sup>) has received the least attention. Hydroxyl ions in hydroxyapatite are most mobile and upon exposure to high temperatures are the first to leave the lattice. Since the surface properties are influenced by the OH<sup>-</sup> content, there is a growing need for the quantification of hydroxyl ions, methods for altering the OH<sup>-</sup> concentration and alignment within the lattice.

Preparation of HA ceramics requires heating that will lead to dehydroxylation (loss of hydroxyl ions). During dehydroxylation, a single water molecule is released from two OH<sup>-</sup> ions. Dehydroxylation introduces vacancies (V) to create oxyhydroxyapatite (OHA; Ca<sub>10</sub>(PO<sub>4</sub>)<sub>6</sub>(OH)<sub>2-2x</sub>O<sub>x</sub>V<sub>x</sub>) with a similar crystal structure to HA [1, 2]. Dehydroxylation can occur over a wide range of temperatures, it depends not only on the composition of the sample, but also on the heating atmosphere. Removal of hydroxyl ions begins at temperatures at about 900 °C in air and 850 °C in a water-free atmosphere [1, 3].

Pure oxyapatite (OAp; Ca<sub>10</sub>(PO<sub>4</sub>)<sub>6</sub>O<sub>x</sub>V<sub>x</sub>) does not contain any hydroxyl ions, but has O<sup>2-</sup> ions and vacancies. As the temperature range for OAp stability is very narrow (around 800-1050 °C) [4, 5] and it easily absorbs moisture from the atmosphere [6], according to the literature all attempts at making a pure OAp have been unsuccessful as the product always contain a small concentration of hydroxyl ions. Heating at excessively high temperature and/or for unnecessarily long durations lead to decomposition of the apatite [3].

A very important property of highly dehydroxylated HA is that it can be easily rehydroxylated in water vapour at a temperature as low as 400 °C [2, 7].

The amount and alignment of hydroxyl ions in HA ceramics influence the bioactivity of this material. Hydroxyl ions in apatite structure enables thermal stability of stoichiometric HA up to 1400 °C [6], improve the structure and surface properties of HA coatings [8], as well as they might have a positive effect on the biological response of HA biomaterials [9].

In this study a highly dehydroxylated OHA was obtained using a crystalline stoichiometric HA as a starting powder. Samples with different hydroxyl concentration were prepared by heating HA at various temperatures in atmosphere containing water. The amount of hydroxyl ions was evaluated by Fourier transform infrared spectroscopy calculating the area of hydroxyl ion absorption line at  $632\text{ cm}^{-1}$  and  $\nu_4\text{ PO}_4^{3-}$  absorption lines.

## Materials and Methods

HA powder was precipitated by neutralizing a calcium nitrate solution ( $\text{Ca}(\text{NO}_3)_2$ ) with ammonium hydrogen phosphate solution ( $(\text{NH}_4)_2\text{HPO}_4$ ) while adjusting the pH with ammonium hydroxide solution ( $\text{NH}_4\text{OH}$ ). The synthesized apatite powder was heated at  $1000\text{ }^\circ\text{C}$  for 15 h in water vapor to provide a high concentration of hydroxyl ions.

OHA with a low amount of  $\text{OH}^-$  in the structure was prepared by heating at high temperature ( $1000\text{ }^\circ\text{C}$ ) for 20 to 45 hours in vacuum ( $1.3 \times 10^{-4}\text{ Pa}$ ). A sorption pump (*Leybold-Heraeus*) was used to provide high vacuum level in a closed quartz system, cylindrical furnace (*LabEc*) was used for heating. Samples were prepared in custom-made quartz ampules, which were flame-cut and closed by fusing after heating at  $1000\text{ }^\circ\text{C}$ . This approach protected the sample from influence of moisture in the ambient atmosphere. The ampule was opened after the sample had reached room temperature.

Different amounts of hydroxyl ions in HA were achieved by rehydroxylating OHA produced in vacuum at  $1000\text{ }^\circ\text{C}$  for 43 h. Thermal gravimetric equipment (*Setaram, Setsys Evolution*) provided a 90% humidity and 10 ml/min gas flow. 90 mg powder sample was put in a Pt crucible and heated up to 350, 400 or  $700\text{ }^\circ\text{C}$  at a heating rate of  $5\text{ }^\circ/\text{min}$ . Dwelling time at maximum temperature was 30 minutes at 350, 400 and  $700\text{ }^\circ\text{C}$  and 1 h at  $400\text{ }^\circ\text{C}$ .

Powder X-ray diffraction (XRD) patterns were recorded on a *D8 Advance diffractometer (Brücker)* using  $\text{Cu K}_\alpha$  radiation ( $\lambda=1.54\text{ \AA}$ ) at 40 kV and 40 mA passing through a  $\text{K}_\beta$  Ni-filter (0.020 mm). The diffracted intensity was recorded over a  $10\text{--}60^\circ$  diffraction angle range ( $2\theta$ ) with a scanning step of  $0.02^\circ$  on a position sensitive detector. All samples were ground with a mortar and pestle before measurement. Crystalline phases were identified using ICDD (International Centre for Diffraction Data) diffraction patterns from pure phases.

A Fourier transform infrared spectrometer (FTIR) *Nicolet Is50 (Thermo Fisher Scientific)* was used to determine functional groups in the samples. Spectra were taken over a  $400\text{--}4000\text{ cm}^{-1}$  range at a resolution of  $4\text{ cm}^{-1}$ . A total of 64 scans were taken and then averaged. Powdered samples were pressed into KBr tablets: a small amount (about 2 mg) of the sample was ground in a mortar, and combined with 200 mg of KBr (*Uvasol<sup>®</sup>, Merck*) by mixing (no grinding) to a homogeneous mixture. Three KBr pellets for each sample were prepared and measured. Deconvolution of the spectral range between  $500\text{ and }700\text{ cm}^{-1}$  was performed using *MagicPlotStudent* software and area of the  $\text{OH}^-$  absorption peak at  $632\text{ cm}^{-1}$  and  $\nu_4\text{ PO}_4^{3-}$  absorption peaks were measured. The  $\text{OH}/\text{PO}_4$  ratio and the percentage of  $\text{OH}^-$  ions were calculated for all samples.

The calcium concentration was measured by atomic absorption spectroscopy with a *contra 300 (AnalytikJena)* spectrophotometer at 442 nm wavelength. Phosphorous was determined as the phosphovanadomolybdate complex with a *UV-1800 (Shimadzu)* spectrophotometer using a wavelength of  $460\text{ cm}^{-1}$ . 6 replicate samples were used and averaged.

## Results and Discussion

The starting HA was highly crystalline, and according to the ICDD database contained all the diffraction peaks corresponding to HA (Fig. 1). The bonding in the thermally modified HA was studied with FTIR spectroscopy. All functional groups represented by absorption peaks in the spectra were characteristic of HA (Fig. 2). Spectra showed a clear hydroxyl vibration peak, at both  $631\text{ cm}^{-1}$  and  $3573\text{ cm}^{-1}$ ; the second peak representing asymmetrical and symmetrical stretching vibrations of adsorbed water was located on a broad band spanning  $2800\text{ cm}^{-1}$  to  $3600\text{ cm}^{-1}$ . The

most intense absorption bands of HA situated at  $1043\text{ cm}^{-1}$  and  $1090\text{ cm}^{-1}$  corresponded to the asymmetric stretching modes of  $\text{PO}_4^{3-}$ , while the peaks at  $962$  and  $472\text{ cm}^{-1}$  arose from the symmetric stretching and bending mode of  $\text{PO}_4^{3-}$ , respectively. The two very sharp and separated peaks at  $601$  and  $573\text{ cm}^{-1}$  represented the bending mode of the phosphate group.

The measured calcium content was  $39.39\pm 0.19\%$ , while phosphorous content was  $18.39\pm 0.12\%$ , which gave the Ca/P molar ratio of 1.66. Detailed previous analysis using thermal gravimetric analysis proved that the HA used in this study is fully hydroxylated and contains 100% hydroxyl ions [10].

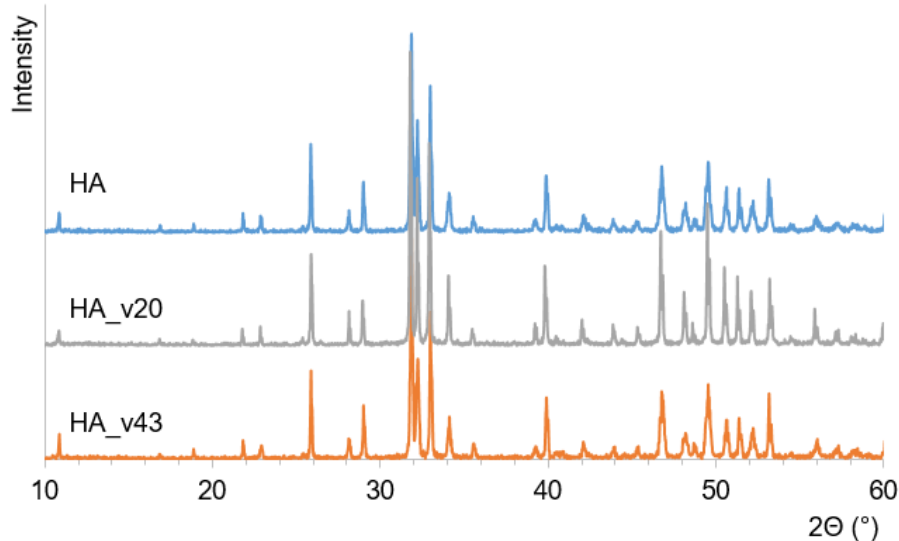


Fig. 1. XRD pattern of the initial HA, and vacuum treated HA (HA\_v20 and HA\_v43)

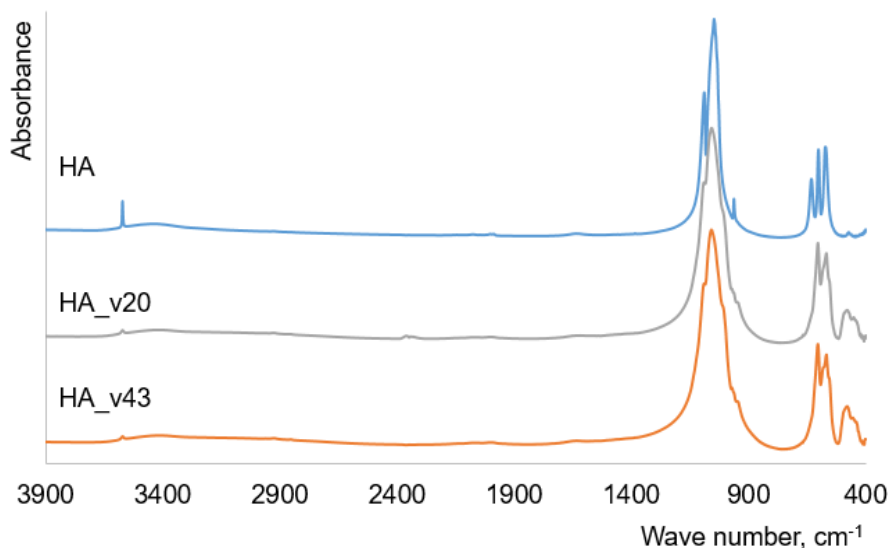


Fig. 2. FTIR spectra of the initial HA, and vacuum treated HA (HA\_v20 and HA\_v43)

To produce OHA with the lowest amount of hydroxyl ions in the structure, namely, with the largest amount of OAp phase, a vacuum in high temperatures provided conditions to favor the removal of hydroxyl ions. As the pure OAp is believed to be unstable and according to the literature has not been obtained, it is important to choose the right heating conditions, so that only the diffusion of hydroxyl ions occurs while maintaining the apatite structure.

OHA with the lowest amount of  $\text{OH}^-$  in the structure was prepared by heating at high temperature ( $1000\text{ }^\circ\text{C}$ ) for 20 or 43 hours in vacuum in a closed quartz system. For 20 h heated HA sample was labeled as HA\_v20 and for 43 h heated HA sample was labeled as HA\_v43. XRD results (Fig. 1) confirmed that the prepared OHA samples retained the apatite structure. FTIR results showed absorption bands characteristic only to apatite (Fig. 2). Traces of  $\text{OH}^-$  absorption bands at  $3570$  and  $632\text{ cm}^{-1}$  and  $\text{PO}_4^{3-}$  band at  $961\text{ cm}^{-1}$  showed the presence of HA phase, while  $\text{PO}_4^{3-}$  absorption

bands at 433, 475 and 945  $\text{cm}^{-1}$  were characteristic of OAp [11, 12]. XRD for all rehydroxylated samples showed no traces of decomposition. FTIR spectra also confirmed HA phase and indicated the presence of OAp.

The 632  $\text{cm}^{-1}$   $\text{OH}^-$  absorption band was chosen for calculating the  $\text{OH}^-$  amount in the products as this band is more sensitive than the absorption band at 3571  $\text{cm}^{-1}$  [13]. The  $\text{OH}^-$  peak was deconvoluted from the phosphate peaks within the 500-700  $\text{cm}^{-1}$  spectral area to enable the measurement of the  $\text{OH}^-$  and  $\text{PO}_4^{3-}$  peak areas.

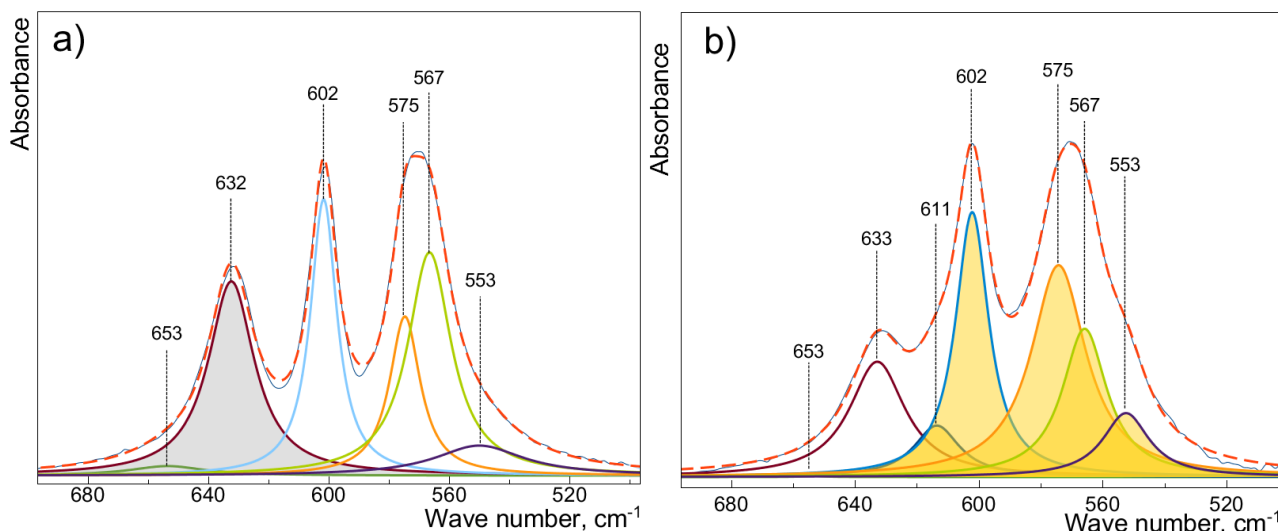


Fig. 3. Deconvoluted FTIR spectra of (a) HA, and (b) OHA (sample: HA\_v43\_reh400-1h). For better visualization,  $\text{OH}^-$  peak area used for further calculations is colored in the figure a, and  $\text{PO}_4^{3-}$  peak area is colored in the figure b

The best fit for deconvolution used 7 Lorentzian curves for the OHA samples (Fig. 3). The absorption peak at 653  $\text{cm}^{-1}$  was assumed to arise from the KBr during sample preparation that could have been introduced from the adsorbed water. The peak at 653  $\text{cm}^{-1}$  was not used for the  $\text{OH}^-$  calculations.

Table 1. Calculated hydroxyl ion content in OHA samples, and information about the absorption peak positions in FTIR spectra range from 500 to 700  $\text{cm}^{-1}$

| Sample name      | Average (OH/ PO <sub>4</sub> ) [a.u.] | OH <sup>-</sup> amount ± stdev [%] | Wavenumber from FTIR spectra [cm <sup>-1</sup> ] |                               |     |     |     |     |
|------------------|---------------------------------------|------------------------------------|--------------------------------------------------|-------------------------------|-----|-----|-----|-----|
|                  |                                       |                                    | OH <sup>-</sup>                                  | PO <sub>4</sub> <sup>3-</sup> |     |     |     |     |
| Start HA         | 0.38                                  | 100                                | 632                                              | -                             | 602 | 575 | 567 | 553 |
| HA_v43_reh700    | 0.37                                  | 98 ± 1                             | 632                                              | -                             | 602 | 575 | 567 | 553 |
| HA_v43_reh400-1h | 0.26                                  | 67 ± 3                             | 633                                              | 611                           | 602 | 575 | 567 | 553 |
| HA_v43_reh400    | 0.22                                  | 59 ± 2                             | 633                                              | 611                           | 602 | 577 | 568 | 553 |
| HA_v43_reh350    | 0.14                                  | 37 ± 2                             | 634                                              | 612                           | 602 | 580 | 568 | 553 |
| HA_v20           | 0.05                                  | 12 ± 1                             | 636                                              | 613                           | 603 | 582 | 568 | 553 |
| HA_v43           | 0.03                                  | 8 ± 1                              | 637                                              | 614                           | 604 | 583 | 568 | 553 |

The analysis of the deconvoluted peaks led to the following findings (Table 1):

- The  $\text{OH}^-$  peak shifts to a higher wavenumber at lower  $\text{OH}^-$  concentrations, *i.e.*, 632  $\text{cm}^{-1}$  for HA with 100%  $\text{OH}^-$  and 637  $\text{cm}^{-1}$  for the sample with the lowest amount of  $\text{OH}^-$ .
- There is an additional  $\text{PO}_4^{3-}$  peak at 611-614  $\text{cm}^{-1}$  for OHA samples (this absorption line was not observed for pure HA samples).
- There is a shift for another  $\text{PO}_4^{3-}$  peak: 575  $\text{cm}^{-1}$  for 100% HA shifts to 583  $\text{cm}^{-1}$  for sample with the largest amount of OAp phase.

A peak shift and broadening occurs with dehydroxylation. A large decrease in wavenumber from  $633\text{ cm}^{-1}$  occurs when larger cations take the place of calcium [14], but this work shows that the absence of  $\text{OH}^-$  ions gives a minor increase in wavenumber. An increase in peak width has been noted when  $\text{OH}^-$  is absent - this could in part be related to an increase in disorder, in agreement with observed FTIR peak broadening in case of low-crystalline apatites [15]. Since both of these changes are marginal, deconvolution is essential to detect these changes. If previously changes in the  $\text{OH}^-$  content were approximated from the  $633\text{ cm}^{-1}$  peak intensity, this work shows a slight increase in wavenumber and an increase in peak width as additional signs to confirm the reduction in  $\text{OH}^-$  content.

## Conclusions

Heating well crystalline hydroxyapatite in a closed quartz system under high vacuum at  $1000\text{ }^\circ\text{C}$  for 43 h produced 90% oxyapatite sample that was stable in air. Oxyhydroxyapatite can be made by rehydroxylating oxyapatite in a humid atmosphere through varying heating temperature and dwelling time. More detailed analysis of FTIR spectra in the  $500\text{-}700\text{ cm}^{-1}$  range showed an increase in the wavenumber of the hydroxyl ion absorption line at  $632\text{ cm}^{-1}$  and phosphate line at  $575\text{ cm}^{-1}$  with increasing the level of dehydroxylation.

## Acknowledgements

We would like to thank A. Krumina from the Institute of Inorganic Chemistry, Riga Technical University for performing part of the XRD measurements. This work has been partly supported by the European Council Seventh Framework Program M-ERA.NET project "Implants signal to bone for bone growth and attachment" Nr. ESRTD/2017/4, and is a topic of investigation in the IRSES Project Nr. 612691 "Refined Step".

## References

- [1] Wang T, Dorner-Reisel A, Müller E. Thermogravimetric and thermokinetic investigation of the dehydroxylation of a hydroxyapatite powder. *Journal of the European Ceramic Society* 2004;24:693-8.
- [2] White AA, Kinloch IA, Windle AH, Best SM. Optimization of the sintering atmosphere for high-density hydroxyapatite-carbon nanotube composites. *Journal of the Royal Society Interface* 2010;7:S529-S39.
- [3] Liao CJ, Lin FH, Chen KS, Sun JS. Thermal decomposition and reconstitution of hydroxyapatite in air atmosphere. *Biomaterials* 1999;20:1807-13.
- [4] Park HC, Baek DJ, Park YM, Yoon SY, Stevens R. Thermal stability of hydroxyapatite whiskers derived from the hydrolysis of  $\alpha$ -TCP. *Journal of Materials Science* 2004;39:2531-4.
- [5] Cihlář J, Buchal A, Trunec M. Kinetics of thermal decomposition of hydroxyapatite bioceramics. *Journal of Materials Science* 1999;34:6121-31.
- [6] Gross KA, Berndt CC, Stephens P, Dinnebier R. Oxyapatite in hydroxyapatite coatings. *Journal of Materials Science* 1998;33:3985-91.
- [7] Tonsuaadu K, Gross KA, Pluduma L, Veiderma M. A review on the thermal stability of calcium apatites. *Journal of Thermal Analysis and Calorimetry* 2012;110:647-59.
- [8] Yang C-W, Lui T-S. Kinetics of hydrothermal crystallization under saturated steam pressure and the self-healing effect by nanocrystallite for hydroxyapatite coatings. *Acta Biomaterialia* 2009;5:2728-37.
- [9] Baxter FR, Bowen CR, Turner IG, Dent ACE. Electrically active bioceramics: A review of interfacial responses. *Annals of Biomedical Engineering* 2010;38:2079-92.
- [10] Pluduma L. Hydroxyl ion quantification in hydroxyapatite and the effect on the biological response. PhD Thesis. Riga: Riga Technical University; 2017.

- [11] Elliott JC. Structure and chemistry of the apatites and other calcium orthophosphates. Elsevier Inc, Amsterdam 1994:387.
- [12] J.C.Trombe. Contribution a l'etude de la decomposition et de la reactivite de certaines apatites hydroxylees et carbonatees. Annales des Chimie 1973;8:251-69.
- [13] Rapacz-Kmita A, Paluszkiewicz C, Slosarczyk A, Paszkiewicz Z. FTIR and XRD investigations on the thermal stability of hydroxyapatite during hot pressing and pressureless sintering processes. Journal of Molecular Structure 2005;744:653-6.
- [14] Engel G, Klee WE. INFRARED-SPECTRA OF HYDROXYL IONS IN VARIOUS APATITES. Journal of Solid State Chemistry 1972;5:28-&.
- [15] Rey C, Combes C, Drouet C, Lebugle A, Sfihi H, Barroug A. Nanocrystalline apatites in biological systems: Characterisation, structure and properties. Materialwissenschaft und Werkstofftechnik 2007;38:996-1002.